frontiers | Frontiers in Photonics

TYPE Original Research
PUBLISHED 09 December 2022
DOI 10.3389/fphot.2022.1071879

Check for updates

OPEN ACCESS

EDITED BY
Katsuaki Tanabe,
Kyoto University, Japan

REVIEWED BY
Santanu Manna,
Indian Institute of Technology Delhi, India
Kenneth Maussang,
Université de Montpellier, France
Martin Kainz,
Vienna University of Technology, Austria

*CORRESPONDENCE
Junqi Liu,
jqliu@semi.ac.cn
Ning Zhuo,
zhuoning@semi.ac.cn
Quanyong Lu,
luqy@baqis.ac.cn

SPECIALTY SECTION
This article was submitted to Terahertz and Microwave Photonics, a section of the journal Frontiers in Photonics

RECEIVED 01 November 2022
ACCEPTED 21 November 2022
PUBLISHED 09 December 2022

CITATION
Li W, Li Y, Ma Y, Xu Y, Liu J, Zhuo N, Lu Q, Wang L, Zhang J, Zhai S, Liu S and Liu F (2022), Continuous-wave terahertz quantum cascade laser based on a hybrid bound to bound quantum design.
*Front. Photonics* 3:1071879.
doi: 10.3389/fphot.2022.1071879

COPYRIGHT
© 2022 Li, Li, Ma, Xu, Liu, Zhuo, Lu, Wang, Zhang, Zhai, Liu and Liu. This is an open-access article distributed under the terms of the Creative Commons Attribution License (CC BY). The use, distribution or reproduction in other forums is permitted, provided the original author(s) and the copyright owner(s) are credited and that the original publication in this journal is cited, in accordance with accepted academic practice. No use, distribution or reproduction is permitted which does not comply with these terms.

# Continuous-wave terahertz quantum cascade laser based on a hybrid bound to bound quantum design

Weijiang Li[1,2], Yuanyuan Li[1,3], Yu Ma[1,2], Yunfei Xu[1,2], Junqi Liu[1,2]*, Ning Zhuo[1]*, Quanyong Lu[3]*, Lijun Wang[1,2], Jinchuan Zhang[1], Shenqiang Zhai[1], Shuman Liu[1,2] and Fengqi Liu[1,2,3]

[1]Key Laboratory of Semiconductor Materials Science, Institute of Semiconductors, Chinese Academy of Sciences, Beijing, China, [2]College of Materials Science and Opto-Electronic Technology, University of Chinese Academy of Sciences, Beijing, China, [3]Division of Quantum Materials and Devices, Beijing Academy of Quantum Information Sciences, Beijing, China

We report a low threshold power density and high power output terahertz quantum cascade laser emitting at ~3.9 THz operating in continuous-wave mode. The high output power and wall-plug efficiency are achieved based on a hybrid bound-to-bound quantum active design. A record output power of 312 mW and a low threshold power density of 0.8 kW/mm$^3$ (threshold current density of 109 A/cm$^2$) in continuous-wave mode at 20 K is demonstrated for a 300-μm-wide and 2-mm-long single-ridge device. The highest wall-plug efficiency is 1.38% and the slope efficiency is 684 mW/A with an internal quantum efficiency of ~120 photons per injected electron. The demonstration of this low-threshold and high-power THz laser will promote THz-based remote sensing and standoff detection for pharmaceutical and health industry applications.

KEYWORDS

**bound to bound transition, continuous-wave mode, semiconductor laser, Terahertz, low threshold power density**

## Introduction

High-power terahertz (THz) sources are highly desired for applications in biomolecular and chemical sensing such as detection of DNA and protein (Cheon et al., 2016), evaluation of pollutants and hazards (Galstyan et al., 2021), and atmosphere monitoring (Miao et al., 2018). THz Quantum cascade lasers (THz QCLs) (Kohler et al., 2002; Williams, 2007; Kumar, 2011; Fei et al., 2021) are one of the most promising terahertz sources for those applications, with a vast commercial potential. Multi-Watt THz QCLs in pulsed mode has been achieved in recent years. Some remarkable results include terahertz QCLs with 24-μm-thick active region embedded into a surface-plasmon waveguide that realized ~2.4 W at 10 K and ~1.8 W at 77 K (Li et al., 2017), phase-locked terahertz plasmonic laser array with 2 W output power in a single spectral mode (Jin et al., 2020), terahertz QC VECSEL (vertical-external-cavity surface-

emitting laser) with peak output powers up to 1.35 W at 6 K and 830 mW at 77 K (Curwen et al., 2018). Typically, the low absorption of water vapor, high imaging resolution and high-power emission in continuous wave (CW) operation is desired in many targeted applications, such as remote imaging and sensing where a significant amount of power is needed (Barbieri et al., 2003; Hubers et al., 2013; Liu et al., 2021). After the rapid development of CW power performance in the early days of THz QCLs (Scalari et al., 2003; Williams et al., 2005; Williams et al., 2006), however, the progress slowed down and the maximum power remained at 138 mW for a long time (Williams et al., 2006). Until 2016, high CW power of 164 mW (Li et al., 2016a) and 230 mW (Wang et al., 2016) were achieved by adopting optimized material growth or device process. In general, there are multiple ways to achieve high output power such as improving the internal quantum efficiency of one module, or enhancing the volume of the active core including the number of modules or the laser area. However, simply increasing the number of cascade periods and the laser area will lead to sever heat accumulation in the active core and result in poor power performance, especially for lasers in CW operation (Curwen et al., 2021).

In this work, we designed a hybrid active structure by tailoring quantum transport process to improve the quantum efficiency and threshold for THz QCLs. Suitably, moderately more cascade active stages are allowed to balance the optical power and thermal accumulation. In this design, high CW power up to 312 mW with a threshold power density as low as 0.8 kW/mm$^3$ is demonstrated for a THz QCL emitting at 3.9 THz at 20 K.

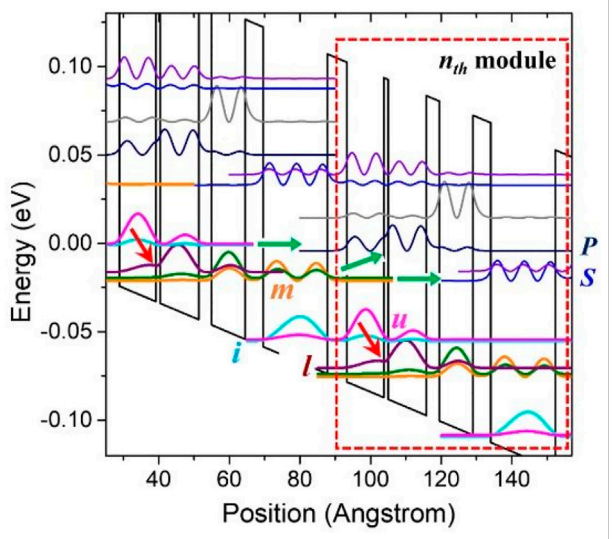


FIGURE 1
Conduction band diagram of a THz QCL with four quantum wells per module in the active region. An electric field of 8.4 kV/cm is applied to this structure. Red arrows represent radiative transitions and green arrows represent parasitic leakage channels.

## Design and fabrication

The active quantum structure is based on a bound-to-bound (BTB) optical transition hybridized with a miniband transportation and phonon-assisted depopulation scheme, as shown in Figure 1. A four-quantum-well quantum design with different oscillator strength can be traced back to reference (Kumar et al., 2006) and (Amanti et al., 2009). The active core is designed with layer thickness in angstrom of **55.1**/103.9/**11.7**/109.2/**37.1**/95.4/**50.9**/(82.3+ 100) at 3.9 THz. GaAs layers are in roman font, $Al_{0.2}Ga_{0.8}As$ are in bold, and the silicon doped layer (n = 4.0×10$^{16}$ cm$^{-3}$) is underlined. In this scheme, electrons are injected into the upper level u from the preceding module injector level I *via* resonant tunneling. Then the lasing occurs through a diagonal transition between the upper level *u* and the lower level *l*. The electron is then serially tunneled from *l* to the miniband level *m*, and depopulated to the ground state *i* through LO-phonon scattering. In this structure, the lower level *l* is largely decoupled with the miniband levels, forming a bound-to-bound (BTB) transition, which in turn favors a stronger gain and a low threshold operation (Wienold et al., 2010). In a THz QCL active region, the parasitic levels with similar energy and location to lasing levels could form carrier leakage channels that deteriorate the internal quantum efficiency. For our BTB design, the leakage channels (Albo and Flores, 2017) between the upper level *u* and parasitic level *P*, the minibands m and parasitic levels *S* and *P*, as the arrows denoted in Figure 1, are largely suppressed. Table 1 lists the calculation parameters of the active region, which was obtained by carrying out an one-dimensional Schrödinger-Poisson solver with numerical transfer Matrix method. Clearly, the normalized oscillation strength *f* for all the three possible leakages between the laser levels and the parasitic levels are small for the BTB design. This is beneficial to achieve a low threshold operation from the BTB design. In addition, a higher aluminum concentration of 20% in barriers was used to reduce the thermally activated leakage of carriers into the continuum or bounded higher-energy levels (Kainz et al., 2018; Khalatpour et al., 2021).

The THz QCL was grown *via* solid source molecular beam epitaxy (SSMBE) on a semi-insulating GaAs substrate. The growth temperature was set as 650°C. The epitaxial layer sequence was as follows: 500 nm highly-doped n$^+$-GaAs layer (Si, n = 3×10$^{18}$ cm$^{-3}$), 300-stage active region, and 100-nm-thick upper highly-doped (Si, n = 5×10$^{18}$ cm$^{-3}$) n$^+$-GaAs layer, leading to an overall thickness of 19.4 μm. Figure 2 shows the calculated and measured high resolution XRD triple-axis 2$\theta$/$\omega$ curves of the wafer. According to the spacing of the satellite peaks, excellent agreement of layer thicknesses with the design values is obtained. The average full-width at half-maximum (FWHM) for the first four satellite peaks is as narrow as 10.7 arcsec, illustrating a good

**TABLE 1 Simulation results of the THz QCL active region (125 K).**

| $\Omega_{iu}$ (meV) | $E_{ul}$ (meV) | $\tau$ (ps) | $f_{ul}$ | $f_{uP}$ | $f_{mS}$ | $f_{mP}$ |
|---|---|---|---|---|---|---|
| 0.3 | 15.9 | 1.6 | 0.47 | 0.0001 | 0.08 | 0.036 |

$\Omega_{iu}$ is the coupling energy between the injector state and the upper state, $E_{ul}$ is the.
Photon energy, $f$ is the normalized oscillator strength, $\tau$ is the lifetime of the upper state.

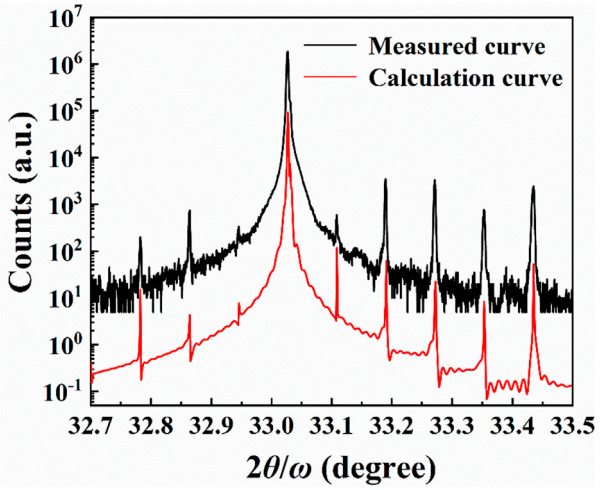


FIGURE 2
High resolution XRD curves from the wafer. The top black curve is the measured result, and the red curve is the calculation result.

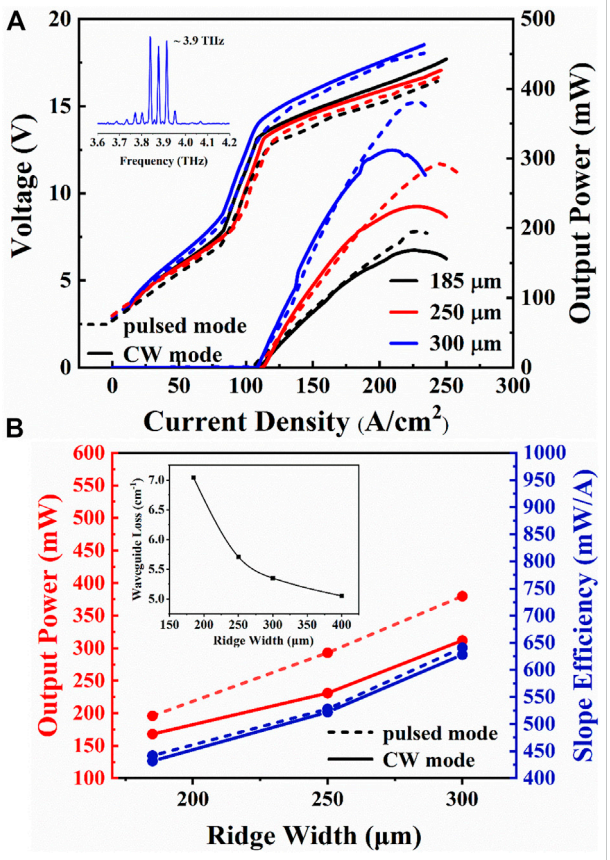


FIGURE 3
**(A)** Power-current density-voltage characteristics of 2-mm-long devices with different ridge widths. The inset shows the cw spectrum of the 300-μm-wide device working at the maximum output power at 20 K. **(B)** The cw power and slope efficiency *versus* ridge width for devices in cw mode. The dash-dotted lines in both figures are for pulsed mode operation and solid lines are for cw mode operation.

growth homogeneity and small interface roughness. The MBE grown wafers were then fabricated into ridge lasers with a single-surface plasmon (SP) waveguide. The optimized manufacture process of devices was as follows: laser ridges spaced 300 μm apart were defined using photolithography and non-selective wet chemical etching ($H_3PO_4$:$H_2O_2$:$H_2O$ = 1:1:10) which stopped above the bottom $n^+$-GaAs contact layer. Ohmic-contact was realized by the deposition of Au/Ge/Ni/Au (26/54/15/150 nm) on the $n^+$-GaAs contact layer followed by fast annealing and the metallization was formed by the evaporation of Ti/Au (5/200 nm). After the substrate being thinned down to 150 μm, a Ti/Au metal layer was deposited for soldering. Then the waveguides were cleaved into 2 mm and high-reflectivity (HR) coating consisting of $Al_2O_3$/Ti/Au/$Al_2O_3$ (200/10/100/120 nm) was deposited on the back facet by electron beam evaporation. Finally, the lasers were mounted epitaxial-side up on copper heat-sinks with indium solder. More details of fabrication progress can be found in Ref. 26.

The fabricated device was mounted into a well-designed home-made cryostat with high refrigeration capacity at 20 K. The spectra were measured by a Fourier transform infrared spectrometer (Bruker, Vertex 80V) with a spectral resolution of 0.25 $cm^{-1}$. When the lasers were operated in CW mode, no modulation was used for the current resource and the emitted powers were measured with a Thomas-Keating-power-meter-calibrated thermopile detector (Li et al., 2016b) while the diameter of the detector aperture is 30 mm. When pulsed currents with repeat frequency of 5 kHz and pulse width of 2 μs were applied on lasers, the output powers were collected by a Winston cone placed near the laser face and tested by a Thomas Keating absolute THz power-meter with a modulation frequency of 20 Hz and a duty cycle of 50%. Furthermore, none of the

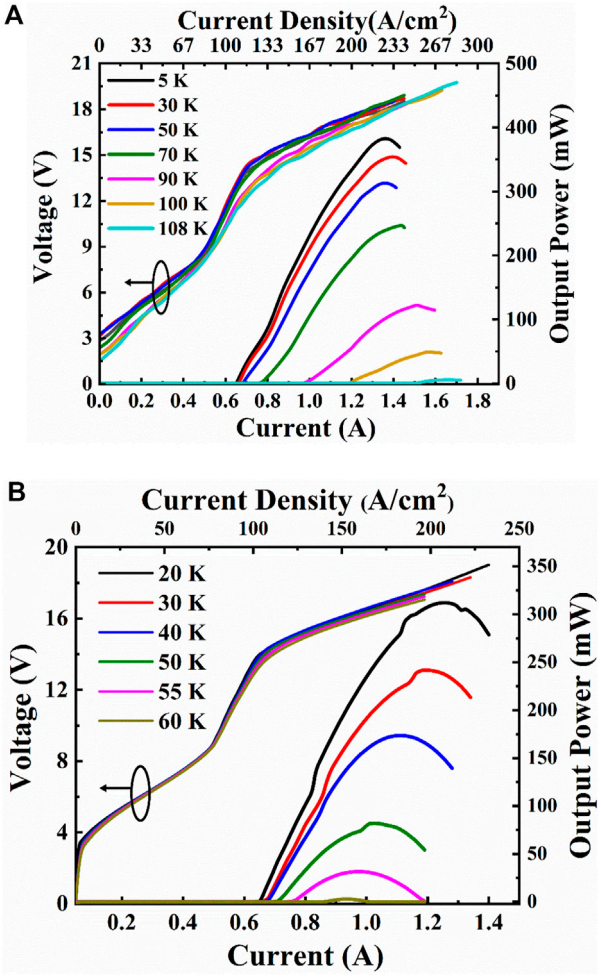


FIGURE 4
The measured electrical and optical characteristics of the 300-μm-wide device operating in **(A)** pulsed mode and **(B)** cw mode at different temperatures.

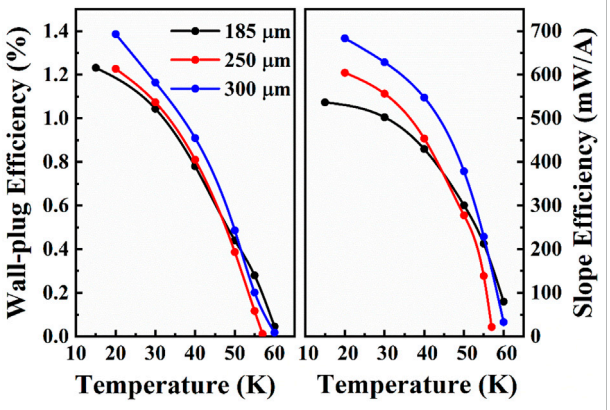


FIGURE 5
The wall-plug efficiency and slope efficiency for devices in cw mode at different heat sink temperatures.

optical powers presented in this paper were corrected by the collection efficiency of the apparatus or the absorption of the cryostat polyethylene windows, despite that the measured output powers of the devices were only ~75% of the total power due to these factors.

## Results and discussion

Figure 3A shows the power-current density-voltage characteristics of three 2-mm-long lasers with different ridge widths at low temperatures. The emitted optical powers of the devices operating in CW mode are plotted in solid lines, and the dot dash lines represent the pulsed output powers at 5 K. As shown in Figure 3A, all three devices have similar threshold current densities (*J*th) ranging from 105 to 112 A/cm$^2$ regardless of working conditions in pulsed or CW modes. The corresponding threshold power density of the 300-μm-wide device is 0.8 kW/mm$^3$, which is about 1/3 of the previous work (2.7 kW/mm$^3$) (Curwen et al., 2021). This low threshold operation is a clear indication of the greatly suppressed carrier leakages in our BTB design. The indistinguishable threshold current densities and slope efficiencies between different operating modes illustrate the sufficient heat dissipation of the active cores in CW mode due to the low *J*th. In this condition, the output powers follow an ultralinear relationship as a function of the ridge widths for devices with the same cavity length, as shown in Figure 3B. This ultralinear behavior is a combined effects of the low threshold active region design and the lower waveguide losses of fundamental mode in wider cavity as plotted in the inset of Figure 3B. At 5 K, the pulsed output powers are 196, 293, and 380 mW, respectively, for devices with ridge widths of 185, 250, and 300 μm. Correspondingly, the CW output powers are 168, 231, and 312 mW at 20 K. In the inset of Figure 3A, the CW emission spectrum of the 300-μm-wide device at the maximum power is shown. The central frequency is ~3.9 THz, which is consistent with the active region design.

Figure 4 shows the measured electrical and optical characteristics of the 300-μm-wide device. In Figure 4A, the output powers as a function of injection currents from the device in pulsed mode are presented. At 5 K, the threshold current (*I*th) and threshold current density are 0.65A and 108.5A/cm$^2$, and the maximum peak output power is 380 mW with a slope efficiency of 668 mW/A. As the heat sink temperature increases, the *I*th and *J*th increase to 1.5A and 250 A/cm$^2$, respectively, and the maximum peak output power is still 5.7 mW at 108 K. The power-current-voltage characteristics of the device operating in CW mode at different heat sink temperatures are exhibited in Figure 4B. At 20 K, the threshold current density is 109 A/cm$^2$, which is close to that of pulsed mode. The maximum CW output power is 312 mW at the input electrical power consumption of 22.5W, and

corresponding wall-plug efficiency is 1.38%. The maximum lasing temperature is 60 K with an output power of 2.7 mW. To further improve the device performance, the epitaxial-down mounting and the anti-reflection coating on the front facet can be employed, which allow for improvement in *J*th and heat-dissipation.

Figure 5 shows the wall-plug efficiencies and slope efficiencies of the three devices in a temperature range from 15 to 60 K in CW operation. At 20 K, the highest wall-plug efficiency of 1.38% is obtained from the 300-μm-wide device. And the maximum slope efficiency of ~684 mW/A is also obtained from this device. According to the expression of slope efficiency

$$\frac{dP}{dI} = \frac{h\nu}{e} N_p \frac{\alpha_m}{\alpha_m + \alpha_w} \eta_i$$

where $h\nu$ is the photon energy, $e$ is the elemental electronic charge, $N_p$ is the number of cascade periods, $\alpha_m = 2.85\ cm^{-1}$ is the mirror loss, $\alpha_w = 5.3\ cm^{-1}$ is the waveguide loss, and $\eta_?$ is the internal quantum efficiency of each period, an internal quantum efficiency of ~120 photons per injected electron is obtained.

## Conclusion

In conclusion, a high-power terahertz quantum cascade laser operating in continuous-wave mode is achieved based on a hybrid bound-to-bound active region design. Under the premise of low-threshold design with suppressed carrier leakage channels, the output powers follow an ultralinear relationship as a function of the ridge widths (≤300 μm) for the 2-mm-long devices. At 20 K, a record-high output power of 312 mW and a low threshold power density of 0.8 kW/mm$^3$ in continuous-wave mode is realized from a 300-μm-wide device. The highest wall-plug efficiency is 1.38% and the slope efficiency is 684 mW/A. Furthermore, the output power of 2.7 mW still can be obtained at 60 K with a threshold current density of 145 A/cm$^2$. The demonstration of this low threshold and high-power THz laser source will open up THz-based remote sensing and standoff detection for pharmaceutical and health industry applications.

## Data availability statement

The raw data supporting the conclusion of this article will be made available by the authors, without undue reservation.

## Author contributions

All authors listed have made a substantial, direct, and intellectual contribution to the work and approved it for publication. The project was supervised by JL. WL and YL performed the device fabrication and characterization and wrote the manuscript. JL, QL carried out the design and involved the data analysis. NZ, LW, and FL performed MBE growth. YM, YX, JZ, SZ, SL participated in device preparation and data analysis.

## Funding

This work was supported by National Natural Science Foundation of China under Grant Nos. 61734006, 61835011, 61991430, 62274014; Key Program of the Chinese Academy of Sciences under Grant Nos. XDB43000000 and QYZDJ-SSW-JSC027; Youth Innovation Promotion Association of the Chinese Academy of Sciences (2021107).

## Acknowledgments

The authors would like to thank Ping Liang for her help in the processing.

## Conflict of interest

The authors declare that the research was conducted in the absence of any commercial or financial relationships that could be construed as a potential conflict of interest.

## Publisher's note

All claims expressed in this article are solely those of the authors and do not necessarily represent those of their affiliated organizations, or those of the publisher, the editors and the reviewers. Any product that may be evaluated in this article, or claim that may be made by its manufacturer, is not guaranteed or endorsed by the publisher.

## References

Albo, A., and Flores, Y. V. (2017). Carrier leakage dynamics in terahertz quantum cascade lasers. *IEEE J. Quantum Electron.* 53 (5), 18500508–8. Art no. doi:10.1109/jqe.2017.2740261

Amanti, M. I., Scalari, G., Terazzi, R., Fischer, M., Beck, M., Faist, J., et al. (2009). Bound-to-continuum terahertz quantum cascade laser with a single-quantum-well phonon extraction/injection stage. *New J. Phys.* 11 (12), 125022. Art. no. 125022. doi:10.1088/1367-2630/11/12/125022

Barbieri, S., Alton, J., Dhillon, S., Beere, H., Evans, M., Linfield, E., et al. (2003). Continuous-wave operation of terahertz quantum-cascade lasers. *IEEE J. Quantum Electron.* 39 (4), 586–591. doi:10.1109/jqe.2003.809328

Cheon, H., Yang, H., Lee, S. H., Kim, Y. A., and Son, J. H. (2016). Terahertz molecular resonance of cancer DNA. *Sci. Rep.* 6, 37103. Art. no. 37103. doi:10.1038/srep37103

Curwen, C. A., Addamane, S. J., Reno, J. L., Shahili, M., Kawamura, J. H., Briggs, R. M., et al. (2021). Thin THz QCL active regions for improved continuous-wave operating temperature. *AIP Adv.* 11 (12), 125018. Art. no. doi:10.1063/5.0071953

Curwen, C. A., Reno, J. L., and Williams, B. S. (2018). Terahertz quantum cascade VECSEL with watt-level output power. *Appl. Phys. Lett.* 113 (1), 011104. Art. no. doi:10.1063/1.5033910

Fei, T., Zhai, S. Q., Zhang, J. C., Zhuo, N., Liu, J. Q., Wang, L. J., et al. (2021). High power λ ~ 8.5 μm quantum cascade laser grown by MOCVD operating continuous-wave up to 408 K. *J. Semicond.* 42 (11), 112301. Art. no. 112301. doi:10.1088/1674-4926/42/11/112301

Galstyan, V., D'Arco, A., Fabrizio, M. D., Poli, N., Lupi, S., and Comini, E. (2021). Detection of volatile organic compounds: From chemical gas sensors to terahertz spectroscopy. *Rev. Anal. Chem.* 40 (1), 33–57. doi:10.1515/revac-2021-0127

Hubers, H. W., Eichholz, R., Pavlov, S. G., and Richter, H. (2013). High resolution terahertz spectroscopy with quantum cascade lasers. *J. Infrared Millim. Terahertz waves* 34, 325–341. doi:10.1007/s10762-013-9973-7

Jin, Y., Reno, J. L., and Kumar, S. (2020). Phase-locked terahertz plasmonic laser array with 2 W output power in a single spectral mode. *Optica* 7 (6), 708–715. doi:10.1364/optica.390852

Kainz, M. A., Schönhuber, S., Andrews, A. M., Detz, H., Limbacher, B., Strasser, G., et al. (2018). Barrier height tuning of terahertz quantum cascade lasers for high-temperature operation. *ACS Photonics* 5 (11), 4687–4693. doi:10.1021/acsphotonics.8b01280

Khalatpour, A., Paulsen, A. K., Deimert, C., Wasilewski, Z. R., and Hu, Q. (2021). High-power portable terahertz laser systems. *Nat. Photonics* 15, 16–20. doi:10.1038/s41566-020-00707-5

Kohler, R., Tredicucci, A., Beltram, F., Beere, H. E., Linfield, E. H., Davies, A. G., et al. (2002). Terahertz semiconductor heterostructure laser. *Nature* 417 (6885), 156–159. doi:10.1038/417156a

Kumar, S. (2011). Recent progress in Terahertz quantum cascade lasers. *IEEE J. Sel. Top. Quantum Electron.* 17 (1), 38–47. doi:10.1109/jstqe.2010.2049735

Kumar, S., Williams, B. S., Hu, Q., and Reno, J. L. (2006). 1.9 THz quantum-cascade lasers with one-well injector. *Appl. Phys. Lett.* 88 (12), 121123. Art. no. 121123. doi:10.1063/1.2189671

Li, L. H., Chen, L., Freeman, J. R., Salih, M., Dean, P., Davies, A. G., et al. (2017). Multi-Watt high-power THz frequency quantum cascade lasers. *Electron. Lett.* 53 (12), 799–800. doi:10.1049/el.2017.0662

Li, Y. Y., Liu, J. Q., Liu, F. Q., Zhang, J. C., Zhai, S. Q., Zhuo, N., et al. (2016). High power-efficiency terahertz quantum cascade laser. *Chin. Phys. B* 25 (8), 084206. Art no. doi:10.1088/1674-1056/25/8/084206

Li, Y. Y., Wang, T., Zhai, S. Q., Liu, J. Q., Liu, F. Q., and Wang, Z. G. (2016). High-power epitaxial-side down mounted terahertz quantum cascade lasers. *Electron. Lett.* 52 (16), 1401–1402. doi:10.1049/el.2016.1802

Liu, L., Weng, C. S., Li, S. L., Husi, L., Hu, S., and Dong, P. Y. (2021). Passive remote sensing of ice cloud properties at terahertz wavelengths based on genetic algorithm. *Remote Sens. (Basel).* 13 (4), 735. doi:10.3390/rs13040735

Miao, X. Y., Zhan, H. L., Zhao, K., Zhang, Z. W., Xu, L., Zhang, C. L., et al. (2018). Terahertz-dependent PM2.5 monitoring and grading in the atmosphere. *Sci. China Phys. Mech. Astron.* 61 (10), 104211. Art. no. 104211. doi:10.1007/s11433-018-9237-1

Scalari, G., Ajili, L., Faist, J., Beere, H., Linfield, E., Ritchie, D., et al. (2003). Far-infrared (λ ≈ 87 μm) bound-to-continuum quantum-cascade lasers operating up to 90K. *Appl. Phys. Lett.* 82 (19), 3165–3167. doi:10.1063/1.1571653

Wang, X. M., Shen, C., Jiang, T., Zhan, Z. Q., Deng, Q. H., Li, W. H., et al. (2016). High-power terahertz quantum cascade lasers with ~0.23 W in continuous wave mode. *AIP Adv.* 6 (7), 075210. Art. no. doi:10.1063/1.4959195

Wienold, M., Schrottke, L., Giehler, M., Hey, R., Anders, W., and Grahn, H. T. (2010). Low-threshold terahertz quantum-cascade lasers based on GaAs/Al0.25Ga0.75As heterostructures. *Appl. Phys. Lett.* 97 (7), 071113. Art. doi:10.1063/1.3480406

Williams, B. S., Kumar, S., Hu, Q., and Reno, J. L. (2006). High-power terahertz quantum cascade lasers. *Electron. Lett.* 42 (2), 89–91. doi:10.1049/el:20063921

Williams, B. S., Kumar, S., Hu, Q., and Reno, J. L. (2005). Operation of terahertz quantum-cascade lasers at 164 K in pulsed mode and at 117 K in continuous-wave mode. *Opt. Express* 13 (9), 3331–3339. doi:10.1364/opex.13.003331

Williams, B. S. (2007). Terahertz quantum-cascade lasers. *Nat. Photonics* 1 (9), 517–525. doi:10.1038/nphoton.2007.166